Dynamic Structure of Vesicle-Bound Melittin in a Variety of Lipid Chain Lengths by Solid-State NMR

Shuichi Toraya, Katsuyuki Nishimura, and Akira Naito
Faculty of Engineering, Yokohama National University, Yokohama, Japan

ABSTRACT Solid-state ^{31}P- and ^{13}C-NMR spectra were recorded in melittin-lecithin vesicles composed of 1,2-dilauroyl-*sn*-glycero-3-phosphocholine (DLPC) or 1,2-dipalmitoyl-*sn*-glycero-3-phosphocholine (DPPC). Highly ordered magnetic alignments were achieved with the membrane surface parallel to the magnetic field above the gel-to-liquid crystalline phase transition temperature (T_c). Using these magnetically oriented vesicle systems, dynamic structures of melittin bound to the vesicles were investigated by analyzing the ^{13}C anisotropic and isotropic chemical shifts of selectively ^{13}C-labeled carbonyl carbons of melittin under the static and magic-angle spinning conditions. These results indicate that melittin molecules adopt an α-helical structure and laterally diffuse to rotate rapidly around the membrane normal with tilt angles of the N-terminal helix being $-33°$ and $-36°$ and those of the C-terminal helix being 21° and 25° for DLPC and DPPC vesicles, respectively. The rotational-echo double-resonance method was used to measure the interatomic distance between [1-^{13}C]Val^{8} and [^{15}N]Leu^{13} to further identify the bending α-helical structure of melittin to possess the interhelical angles of 126° and 119° in DLPC and DPPC membranes, respectively. These analyses further lead to the conclusion that the α-helices of melittin molecules penetrate the hydrophobic cores of the bilayers incompletely as a pseudo-*trans*-membrane structure and induce fusion and disruption of vesicles.

INTRODUCTION

Melittin is a major component of venom of a honeybee, *Apis mellifera*, consisting of 26 amino acid residues with the primary structure of GIGAVLKVLTTGLPALISWIKRKRQQ-NH_2 (Habermann and Jentsch, 1967). Melittin disrupts biomembranes and artificial lipid membranes (Habermann, 1972; Sessa et al., 1969) and promotes phospholipid hydrolysis catalyzed by phospholipase A_2 (Mollay and Kreil, 1974; Mollay et al., 1976). Furthermore, melittin induces fusion of phospholipid vesicles (Morgan et al., 1983; Eytan and Almary, 1983). It was shown by electron microscopy with a freeze-fracture method that melittin induces fusion of membranes above the gel-to-liquid crystalline phase-transition temperature, T_c, and membrane disruption with forming discoidal membrane fragments whose edges are surrounded by melittin molecules below T_c in a melittin-lecithin membrane system (Dufourcq et al., 1986). As acyl chain length is increased, the disk tends to be destabilized (Faucon et al., 1995). Melittin has a voltage-dependent ion channel activity across a lipid bilayer (Tosteson and Tosteson, 1981; Kempf et al., 1982), so that melittin was occasionally regarded as a pore-forming peptide by oligomerization.

Three-dimensional structures of melittin have so far been studied under various conditions. In an aqueous medium, monomeric melittin takes random-coil conformation, whereas it mainly adopts an α-helical structure with increasing concentration of NaCl, thereby associating with the peptides to form a tetramer (Talbot et al., 1979). The helicity and tetramerization of melittin in an aqueous solution depend on the concentration of melittin, the ionic strength, and pH (Bello et al., 1982; Quay and Condie, 1983). In a crystalline state, two crystal polymorphs with the space groups of $P6_122$ and $C222_1$ were reported for melittin (Anderson et al., 1980). X-ray structural analyses showed that melittin adopts a similar α-helical structure and bends at the region of $T^{11}G^{12}$ with the kink angle of $\sim 120°$ in both of the crystals: the peptides form a tetramer, where the hydrophilic side chains extend mainly toward the outside of the bend and the hydrophobic sides face the center (Terwilliger and Eisenberg, 1982; Terwilliger et al., 1982). The kink angle between two helical rods, I^2-T^{11} and L^{13}-Q^{26}, of melittin in methanol, is larger than the kink angles found in the crystals (Bazzo et al., 1988). In membrane environments, melittin adopts an α-helical structure when it binds to a sodium dodecylsulfate micelle as shown by circular-dichroism spectra (Dawson et al., 1978; Knöppel et al., 1979), and binds to dodecylphosphocholine micelles with the α-helical axis parallel to the micelle/water interface (Inagaki et al., 1989). Transferred nuclear Overhauser enhancement analysis indicated divergent conformations for the region R^{22}-Q^{26} of melittin bound to lipid bilayers (Okada et al., 1994).

To reveal the mechanisms of the actions of melittin upon lipid bilayers, it has been discussed that the α-helical axis of the peptide orients perpendicularly (Vogel et al., 1983; Brauner et al., 1987) or parallel (Altenbach et al., 1989) to the bilayer plane depending on the types of experiments. The structure of melittin bound to mechanically oriented ditetradecylphosphatidylcholine (DTPC) membrane has been examined by observing the ^{13}C-NMR spectra. The results indicated that melittin takes *trans*-membrane helix and the structure is found to be similar to that found in methanol with the interhelical angle of 160° (Smith et al., 1994). On the other hand, a ''toroidal'' model was proposed

Submitted May 21, 2004, and accepted for publication August 20, 2004.
Address reprint requests to Akira Naito, E-mail address: naito@ynu.ac.jp.

0006-3495/04/11/3323/13 $2.00
doi: 10.1529/biophysj.104.046102

for the pore-forming mechanism, based on information that both the orientations exist for membrane-bound melittin molecules (Yang et al., 2001). Many attempts have been performed to elucidate the mechanism of the interaction between melittin and the membranes. However, information obtained from most of the spectroscopic studies in the structural biology has been limited to analyze structures of melittin bound to membranes under the conditions where the peptide does not exhibit fusion or disruption activities on membranes partly because the samples were less hydrated. It was shown by optical microscopic observations under the excess hydration condition that giant vesicles are formed in 1,2-dimyristoyl-*sn*-glycero-3-phosphocholine (DMPC) bilayer systems containing melittin or dynorphin A(1–17) at a temperature higher than T_c, where the peptides induces membrane fusion (Naito et al., 2000, 2002).

In the presence of the strong magnetic field, the membrane plane of the giant vesicle spontaneously orients parallel to the magnetic field above T_c because the spontaneous orientation is stabilized by the interaction energy between anisotropy of the magnetic susceptibility of the phospholipid molecule and the magnetic field. The vesicle thus undergoes elongation along the magnetic field to increase the orientation energy. Since the hydrated membrane is flexible, melittin molecules can have a dynamic structure. Using solid-state NMR with the oriented melittin-DMPC bilayer system, it was elucidated that melittin adopts a bent *trans*-membrane α-helical structure and laterally diffuses in the membrane with tilting the helical axes to the membrane normal by 30° and 10° for the N- and C-terminal helical axes, respectively. However, the interhelical angle was not determined to be either 160° or 140° above T_c because the signs of the tilt angles could not be determined (Naito et al., 2000).

In this study, the influence of altering length of the lipid acyl chain on the membrane-bound structure of melittin was investigated under the fusion condition above T_c to understand the action of the melittin-inducing membrane fusion and disruption. We analyzed the dynamic structure of melittin bound to vesicles composed of 1,2-dilauroyl-*sn*-glycero-3-phosphocholine (12:0/12:0-phosphatidylcholine; DLPC) or 1,2-dipalmitoyl-*sn*-glycero-3-phosphocholine (16:0/16:0-phosphatidylcholine; DPPC) using solid-state ^{31}P- and ^{13}C-NMR spectroscopies. We also report a novel approach to determine a high-resolution dynamic structure of melittin bound to the membranes under the fusion condition (above the T_c) in view of the ^{13}C chemical shift tensors of the carbonyl carbons.

MATERIALS AND METHODS

Sample preparation

Syntheses of 9-fluorenylmethoxycarbonyl (Fmoc) [1-^{13}C]-L-amino acids were carried out with *n*-(9-fluorenylmethoxycarbonyl)succinimide (Watanabe Chemical Industries, Hiroshima, Japan) and [1-^{13}C]-labeled amino acids (Cambridge Isotope Laboratories, Andover, MA), following the method reported by Paquet (1982). Selectively ^{13}C-labeled melittin molecules at the carbonyl carbon of Gly^3, Ala^4, Val^5, Leu^{16}, Ile^{17}, or Ile^{20} were synthesized using an Applied Biosystems (Foster City, CA) 431A peptide synthesizer with Fmoc solid phase chemistry. The crude peptide yielded by a cleavage reaction of the peptide-resin with Reagent K (Kings et al., 1990) was purified by a reverse-phase high-performance liquid chromatography.

DLPC and DPPC were purchased from Sigma (St. Louis, MO) and used without further purification. Powder of the total amount of 50 mg comprising melittin and DLPC or DPPC with the peptide/lipid molar ratio of 1:10 was dissolved in 9 ml of chloroform with a small amount of methanol. The solvent was subsequently evaporated in vacuo to prepare a homogeneous film, followed by removal of the residual solvent under high vacuum. A freeze-and-thaw cycle was repeated 30 times after the film was swelled with 300 μl of Tris buffer (20 mM Tris, 100 mM NaCl, pH 7.5). Five-millimeter O.D. glass and zirconia tubes were filled with the sample and sealed hermetically. These samples were used for NMR measurements of the melittin-lecithin bilayer systems in the highly hydrated states.

The hydrated membrane dispersion was allowed to stand in the liquid-crystalline state for 1 h. Subsequently, the sample was frozen rapidly so that membrane disruption was not induced by melittin. This frozen sample was lyophilized to retain the structure in the lipid bilayer. The lyophilized powder was placed into a 5-mm O.D. zirconia tube and subsequently used for measuring the principal values of the ^{13}C chemical shift tensor of the ^{13}C-labeled carbonyl carbon and the ^{13}C-^{15}N interatomic distance in the immobile state.

NMR measurements

The ^{31}P- and ^{13}C-NMR measurements were performed on a Chemagnetics CMX infinity-400 NMR spectrometer (Chemagnetics, Fort Collins, CO) operating at the ^{31}P and ^{13}C resonance frequencies of 161.15 and 100.11 MHz, respectively. In the ^{31}P- and ^{13}C-NMR experiments of the hydrated melittin-lecithin membrane dispersions, the free induction decay signals were obtained after 90°-excitation pulses of 5.0- and 5.5-μs widths under the presence of high-power proton decoupling pulses of 50- and 45-kHz amplitudes with the repetition times of 2 and 5 s, respectively. Lorentzian line broadenings of 60, 100, and 30 Hz were applied to the free-induction decay to obtain ^{13}C-NMR spectra under the static, slow magic-angle spinning (slow MAS, spinning frequency of 100 Hz) and magic-angle spinning (MAS, spinning frequency of 2 kHz) conditions before Fourier transformations, respectively. To determine the ^{13}C chemical shift tensors and the interatomic distances, ^{13}C-NMR spectra of the lyophilized powder samples were measured at 0°C using cross-polarization (CP) and magic-angle spinning (MAS) with the contact time of 1 ms and the spinning frequencies of 2 kHz. The principal values of ^{13}C chemical shift tensors of the carbonyl carbons were determined by comparing the sideband patterns obtained in the CP-MAS experiments with the simulated spectra. ^{31}P and ^{13}C chemical shift values were externally referred to 0 ppm for the phosphorus of 85% H_3PO_4 and 176.03 ppm for the carboxyl carbon of glycine from that for tetramethylsilane, respectively. The ^{15}N rotational-echo double-resonance (REDOR) spectra were measured using a *xy*-4 irradiation pulse to compensate the errors of flip angle, off-resonance effect, and fluctuation of RF field for ^{13}C nuclei. The lengths of π-pulses for ^{13}C and ^{15}N nuclei were 12.3 and 13.5 μs, respectively, and the proton decoupling amplitude was 65 kHz. The rotor frequency was controlled to 4000 $\pm$2 Hz. REDOR and full-echo spectra were recorded at various *NcTr* values from 6 to 24 ms, where *Nc* and *Tr* are the rotor cycle and rotor period numbers, respectively. The REDOR differences were evaluated as

$$\Delta S/S_0 = (S_{\text{full echo}} - S_{\text{REDOR}})/S_{\text{full echo}}, \quad (1)$$

where S_{REDOR} and $S_{\text{full echo}}$ are the peak intensities of REDOR and full-echo spectra, respectively. These REDOR differences were plotted against the

NcTr values to fit the theoretically obtained curves to determine the ^{13}C–^{15}N interatomic distance.

RESULTS

Magnetic orientation of melittin-DLPC and melittin-DPPC vesicles

Fig. 1 shows temperature variations of ^{31}P-NMR spectra of the melittin-DLPC and melittin-DPPC bilayers in the hydrated dispersion systems. The ^{31}P-NMR signals for both systems appeared at 0 ppm below T_c of pure lecithins (T_c = 0°C for DLPC, T_c = 41.5°C for DPPC; see Van Dijck et al., 1976), indicating that the bilayer systems were disrupted to form small discoidal particles as reported by electron microscopy (Dufourcq et al., 1986). When the temperature is increased to $\sim T_c$, powder patterns appeared in the ^{31}P-NMR spectrum of the melittin-DLPC bilayers, indicating that the small particles fuse to form larger vesicles. At temperatures $>T_c$, signals became sharp and the chemical shifts were the same as those of the perpendicular components of the axially symmetric ^{31}P chemical-shift powder patterns. It was therefore found that the membrane planes of the vesicles composed of respective DLPC and DPPC orient parallel to the static magnetic field above T_c, to form elongated vesicles in the same manner as melittin-DMPC bilayer systems (Naito et al., 2000). We refer to these magnetically oriented vesicle systems as *MOVS*.

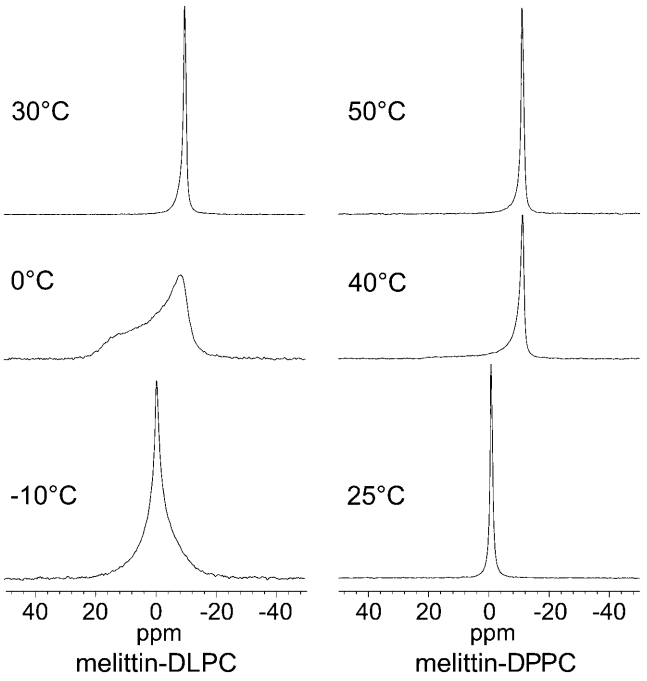

FIGURE 1 Temperature variations of ^{31}P-NMR spectra of the melittin-DLPC and melittin-DPPC bilayers in the hydrated dispersion systems. 1000 transients were accumulated for each spectrum.

Temperature variation of ^{13}C-NMR spectra of melittin-DLPC and melittin-DPPC bilayer systems

Fig. 2 shows temperature variations of ^{13}C-NMR spectra of hydrated melittin-DPPC bilayers recorded under the static condition. Melittin molecules were singly ^{13}C-labeled at carbonyl carbons of Ala^4 and Leu^{16} in the N- and C-terminal helices, respectively. Spectra were recorded under the static condition except for those shown at the bottom of Fig. 2. Sanders et al., have assigned ^{13}C-NMR signals of bicelles consisting of DMPC and DHPC in the magnetic field. They found that the signal of CO_1 (carbonyl carbon in the 1-position of the glycerole of DMPC) shifts upfield from that of CO_2 (carbonyl carbon in the 2-position of the glycerol of DMPC) as the acyl chains orients perpendicularly to the magnetic field (Sanders, 1993). In the melittin-DPPC bilayer system at 50°C, the ^{13}C-NMR signals observed at 174.0 and 168.0 ppm were therefore attributed to CO_2 (denoted ‡) and CO_1 (denoted †) of DPPC, respectively, the same as the case of magnetically oriented bicelle. This result as well as the ^{31}P-NMR spectrum obtained at 50°C indicates that melittin-DPPC membrane planes orient parallel to the magnetic field.

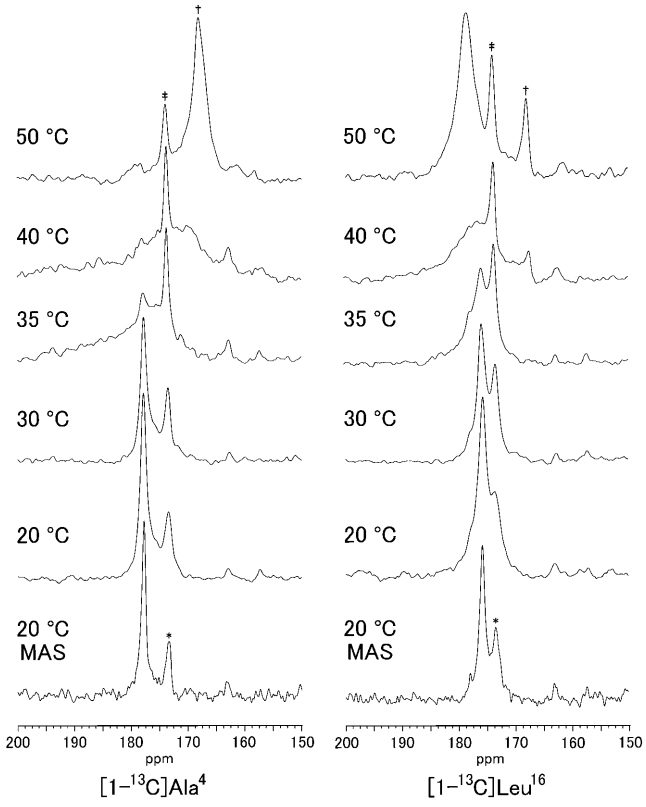

FIGURE 2 Temperature variations of ^{13}C-NMR spectra of [1-^{13}C]Ala^4 and [1-^{13}C]Leu^{16}-melittin bound to hydrated DPPC bilayer under the static condition. The signals denoted by † and ‡ were assigned to the CO_1 and CO_2 of DPPC in the oriented state, respectively. The spectra in the bottom are measured at 20°C under the MAS condition with the spinning frequency of 2 kHz. The signal denoted by * represents the isotropic signal of the carbonyl carbons of the lipid. 4416–18,360 transients were accumulated for the spectra.

The signal intensity of CO_1 (167.3 ppm) decreased at 40°C, and CO_1 and CO_2 signals merged into one peak at 173.8 ppm (denoted *) below 30°C, indicating that the lipid bilayers were disrupted.

At 50°C, relatively narrow signals of [1-^{13}C]Ala^4 and [1-^{13}C]Leu^{16} appeared at 167.7 and 178.5 ppm, respectively. The signals of both [1-^{13}C]Ala^4 and [1-^{13}C]Leu^{16} were broadened at 40°C, and at 35°C, co-existing narrow signals of [1-^{13}C]Ala^4 and [1-^{13}C]Leu^{16} were observed at 177.9 and 175.9 ppm, respectively. At 30°C, the narrow signals of [1-^{13}C]Ala^4 and [1-^{13}C]Leu^{16} appeared at 178.0 and 175.7 ppm, respectively, which were different from the chemical shift values of the melittin molecules bound to the oriented membranes at 50°C. These results indicate that melittin molecules also orient along the magnetic field by strongly binding to the lipid bilayers. In the ^{13}C-NMR spectra of the melittin-DPPC bilayer systems measured at 20°C under the MAS condition (spinning frequency of 2 kHz), the isotropic signals of [1-^{13}C]Ala^4 and [1-^{13}C]Leu^{16} appeared at 177.9 and 175.7 ppm, respectively, as shown in the bottom of Fig. 2. Since the isotropic values under the MAS condition were nearly identical to the chemical-shift values of the narrow peak obtained below 30°C under the static condition, it is apparent that melittin molecules undergo an isotropic motion as a result of formation of small membrane fragments below 30°C. ^{13}C isotropic chemical shift values of [1-^{13}C]Ala^4 and [1-^{13}C]Leu^{16} were 177.3 and 175.8 ppm at 50°C under the MAS condition, respectively (see Table 1). These values are the same as those in the disruption state (below T_c). Therefore, these results suggest that melittin is strongly bound to the membrane fragment in the disruption state with adopting structure similar to that in the vesicle.

Fig. 3 shows temperature variation of ^{13}C-NMR spectra of hydrated melittin-DLPC bilayers recorded under the static condition. Melittin molecules were singly ^{13}C-labeled at the carbonyl carbons of Ala^4 and Leu^{16} in the N- and C-terminal helices, respectively. In the melittin-DLPC bilayer system at 30°C, the signals observed at 174.2 and 168.3 ppm were attributed to CO_2 (denoted ‡) and CO_1 (denoted †) of DLPC, respectively, following the results for bicelles (Sanders, 1993). This result as well as the ^{31}P-NMR spectrum obtained at 30°C indicates that melittin-DLPC membrane planes orient parallel to the magnetic field. For melittin, the signals of the carbonyl carbons of [1-^{13}C]Ala^4 and [1-^{13}C]Leu^{16}-melittin molecules appeared at 169.6 and 175.4 ppm at 30°C, respectively. The signals of both [1-^{13}C]Ala^4 and [1-^{13}C]Leu^{16} were broadened as the temperature was decreased. At 0°C, the signals of the lipid appeared at 173.8 ppm, which is identical to the isotropic chemical shift value, although the signals of [1-^{13}C]Ala^4 and [1-^{13}C]Leu^{16} were significantly broadened.

Since the spectra of [1-^{13}C]Ala^4 and [1-^{13}C]Leu^{16}-melittin molecules in both the membrane systems behave in a similar manner of motional average on the temperature variations across the T_c under the static condition, both the N- and C-terminal regions of melittin molecules strongly interact with the vesicles and the membrane fragments. It is also noticed that free melittin molecules do not exist in the lecithin-melittin dispersion systems because sharp signals of melittin do not appear in the spectra at temperatures higher than T_c.

^{13}C-NMR spectra of melittin bound to magnetically oriented DLPC and DPPC vesicles in the magnetic field

Fig. 4 shows ^{13}C-NMR spectra of a variety of singly [1-^{13}C]-labeled melittin molecules bound to hydrated DLPC bilayers. All of the ^{13}C-NMR measurements in the left column were performed at 30°C under the static condition where the bilayer planes oriented parallel to the magnetic field. ^{13}C chemical shift values, δ_{obs}, of the signals from each carbonyl carbon of the oriented membrane-bound melittin were investigated under the static condition. Thus δ_{obs} at Gly^3, Ala^4, Val^5, Leu^{16}, Ile^{17}, and Ile^{20} were determined as summarized in Table 1. It is noticed that large differences are seen among the values of each residues. The right column of Fig. 4 demonstrates the ^{13}C-NMR spectra at 30°C under the MAS condition with the spinning frequency of 2 kHz.

TABLE 1 ^{13}C chemical shift values of melittin bound to magnetically oriented DLPC and DPPC vesicles

	δ_{iso} ppm*		Structure*		δ_{obs}/ppm		$\Delta\delta$/ppm†		δ_{11}/ppm‡		δ_{22}/ppm‡		δ_{33}/ppm‡		δ^*_{iso}/ppm*‡	
	DLPC	DPPC	DLPC	DPPC	DLPC	DPPC	DLPC	DPPC	DLPC	DPPC	DLPC	DPPC	DLPC	DPPC	DLPC	DPPC
[1-^{13}C]Gly^3	172.6	172.5	α-helix	α-helix	179.4	181.1	−20.4	−25.8	242.5	242.5	180.5	178.5	94.0	96.0	172.3	172.1
[1-^{13}C]Ala^4	177.9	177.3	α-helix	α-helix	169.6	167.7	24.9	28.8	247.5	242.5	189.5	193.5	93.5	94.5	177.3	176.7
[1-^{13}C]Val^5	175.1	175.1	α-helix	α-helix	177.0	179.1	−5.7	−12.0	248.0	244.5	193.0	192.5	85.5	89.0	175.5	175.2
[1-^{13}C]Leu^{16}	175.8	175.8	α-helix	α-helix	175.4	178.5	1.2	−8.1	245.0	245.0	193.0	193.0	89.5	89.5	175.9	175.9
[1-^{13}C]Ile^{17}	175.4	174.8	α-helix	α-helix	168.6	166.6	20.4	24.6	247.0	247.0	189.5	189.5	88.0	88.0	174.7	174.8
[1-^{13}C]Ile^{20}	174.7	174.8	α-helix	α-helix	170.9	172.6	11.4	6.6	244.5	244.0	192.5	192.5	89.0	89.0	175.1	175.2

Measurements of melittin-DLPC and melittin-DPPC bilayer systems were performed at 30°C and 50°C, respectively.

*Typical ^{13}C chemical shift values of δ_{iso} of α-helix and δ_{iso} of β-sheet are 171.6, 168.5; 176.4, 171.8; 174.9, 171.8; 175.7, 170.5; and 174.9, 172.7 for [1-^{13}C]Gly, [1-^{13}C]Ala, [1-^{13}C]Val, [1-^{13}C]Leu, and [1-^{13}C]Ile, respectively (Saitô and Ando, 1989); error ranges of δ_{iso} values were ±0.1 ppm.

†$\Delta\delta = 3(\delta_{iso} - \delta_{obs})$, where $\delta_{obs} \equiv \delta_\perp$; error ranges of $\Delta\delta$ and δ_{obs} values were ±0.6 and ±0.1 ppm, respectively.

‡δ^*_{iso}, δ_{11}, δ_{22}, and δ_{33} values were obtained from CP-MAS measurements of the lyophilized powder samples at 0°C; error ranges of δ^*_{iso}, δ_{11}, δ_{22}, and δ_{33} values were ±0.1, ±1.0, ±1.0, and ±1.0 ppm, respectively.

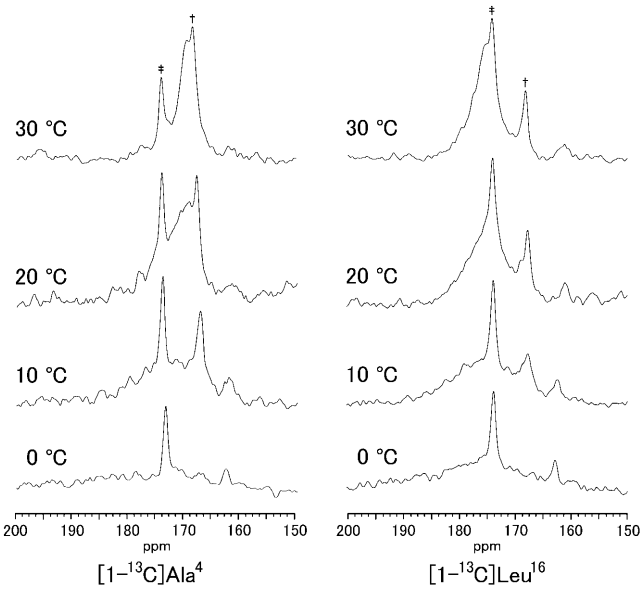

FIGURE 3 Temperature variations of ^{13}C-NMR spectra of [1-^{13}C]Ala^4 and [1-^{13}C]Leu^{16}-melittin bound to hydrated DLPC bilayer under the static condition. Ala^4 and Leu^{16} are present in the N-terminal and C-terminal helices of melittin, respectively. The signals denoted by † and ‡ were assigned to the CO_1 and CO_2 of DLPC in the oriented state, respectively. 5680–13,000 transients were accumulated for the spectra.

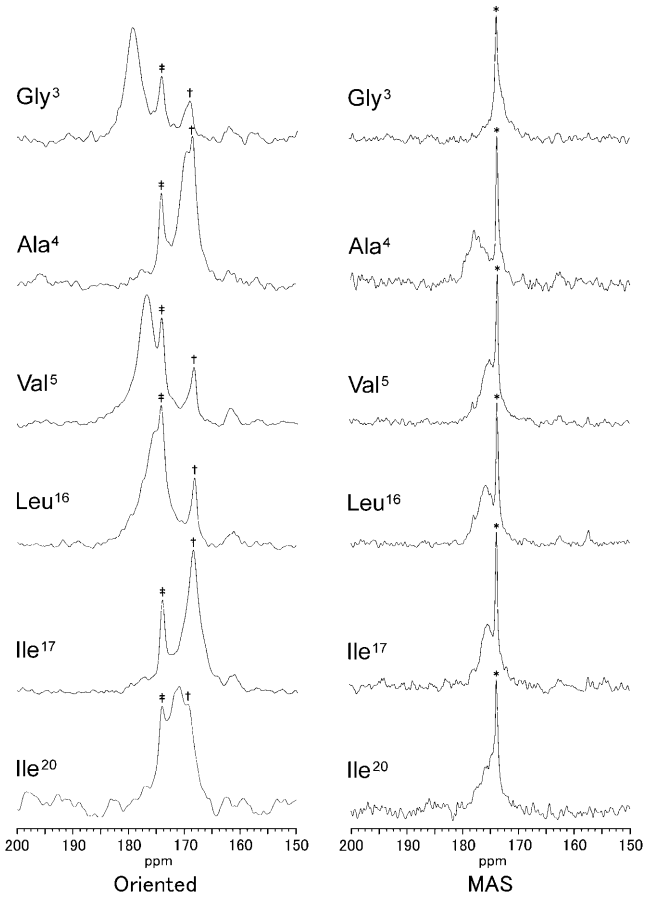

FIGURE 4 ^{13}C-NMR spectra of hydrated melittin-DLPC vesicles at 30°C under the static (*left*) and the MAS (*right*) conditions. A variety of carbonyl carbons were labeled with ^{13}C nuclei. The symbols for the lipid signals are identical in meaning with those defined in Fig. 2. 7900–27,852 transients were accumulated for the spectra.

Conformation-dependent ^{13}C isotropic chemical shift values have been well correlated to the secondary structures in model peptides (Saitô and Ando, 1989). Using the relation, the isotropic chemical shifts, δ_{iso}, revealed that the vicinity of Gly^3, Ala^4, Val^5, Leu^{16}, Ile^{17}, and Ile^{20} adopts α-helical conformations, and hence the overall structure of melittin bound to the DLPC membrane was found to be α-helical (see Table 1).

The left column of Fig. 5 shows ^{13}C-NMR spectra of a variety of singly [1-^{13}C]-labeled melittin molecules bound to the magnetically oriented DPPC bilayers at 50°C. Under the static condition, δ_{obs} values at Gly^3, Ala^4, Val^5, Leu^{16}, Ile^{17}, and Ile^{20} were determined as summarized in Table 1. It is noticed that these values are significantly different from those at respective residues of the melittin in DLPC bilayers. This result indicates that the orientation of melittin helix in DPPC vesicles is slightly different from that in DLPC vesicles. Under the MAS condition, δ_{iso} at each residue was nearly equal to the isotropic chemical shift value obtained in the melittin-DLPC bilayer system. It was therefore found that melittin molecules bound to the DPPC bilayers also adopt an α-helical structure over the entire region.

As demonstrated in our previous study, the carbonyl peaks of melittin bound to magnetically oriented membranes coincide with the perpendicular components of axially symmetric powder patterns obtained under the slow MAS (spinning frequency of 100 Hz) condition. This experiment was performed to disturb the magnetic orientation to observe powder patterns in the NMR spectra. The results indicate that the chemical shifts under the static condition are the same as those of the perpendicular components of the axially symmetric powder pattern obtained from the slow MAS experiments. Therefore, it is classified that melittin laterally diffuses in the membrane with rotating about an axis that is perpendicular to the membrane plane, implying that the rotation axis is perpendicular to the magnetic field (Naito et al., 2000).

In the present experiments, the carbonyl peaks under the oriented conditions in both the DLPC and DPPC membrane systems coincided with the perpendicular components, resonating at $\delta_\perp$, of the axially symmetric powder patterns as shown in Fig. 6. Consequently, it was found that melittin molecules bound to DLPC and DPPC membranes rotate about the axis perpendicular to the membrane plane. It is stressed that the significant difference in δ_{obs} between the melittin-DLPC and melittin-DPPC bilayer systems at each residue were detected as summarized in Table 1. Since it turned out that δ_{obs} is equal to $\delta_\perp$, the change of ^{13}C chemical shift anisotropies, $\Delta\delta = \delta_{\|}$–$\delta_{obs} = 3(\delta_{iso}$–$\delta_{obs})$, of melittin

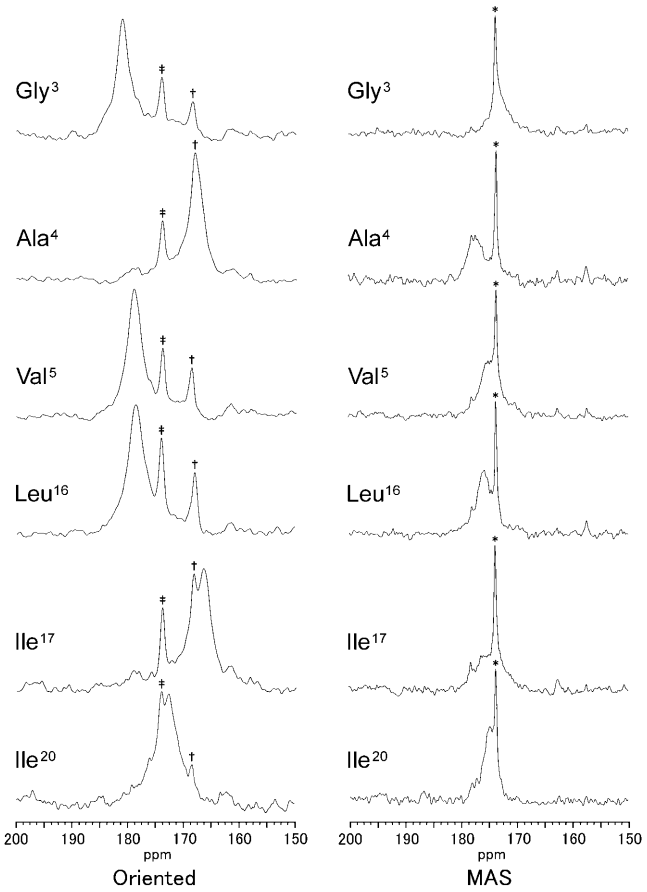

FIGURE 5 ^{13}C-NMR spectra of hydrated melittin-DPPC vesicles at 50°C under the static (*left*) and the MAS (*right*) conditions. A variety of carbonyl carbons were labeled with ^{13}C nuclei. The symbols for the lipid signals are identical in meaning with those defined in Fig. 2. 7000–30,000 transients were accumulated for the spectra.

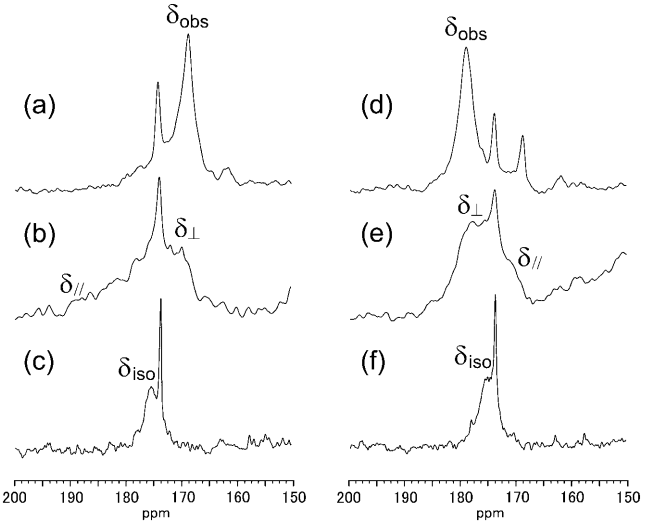

FIGURE 6 ^{13}C-NMR spectra of hydrated [1-^{13}C]Ile^{17}-melittin-DLPC (*left*) and [1-^{13}C]Val^{5}-melittin DPPC (*right*) vesicle systems under the static (*a* and *d*; oriented), slow MAS (*b* and *e*; spinning frequency of 100 Hz), and MAS (*c* and *f*; spinning frequency of 2 kHz) conditions. 15,856–31,744 transients were accumulated for the spectra.

bound to the differently oriented membranes, actually depends on the orientation of melittin molecules in membranes with the different acyl chain lengths.

^{13}C-NMR spectra of melittin in the lyophilized lecithin bilayer system

To determine the principal values of the ^{13}C chemical shift tensor without motional averaging for each carbonyl carbon of melittin bound to the lecithin bilayer, ^{13}C-NMR spectra of the lyophilized powder samples of the melittin-lecithin bilayer systems were measured using cross-polarization and magic-angle spinning (CP-MAS) with the spinning frequency of 2 kHz (Fig. 7). Since membrane disruption can be induced in the processes of freezing and melting, lyophilization was carried out after rapid freezing by use of the liquid nitrogen. The isotropic chemical shift values, δ^{*}_{iso}, obtained from the lyophilized powder samples were almost identical with δ_{iso} obtained from the hydrated bilayer dispersion systems at the respective carbonyl carbons, implying that the α-helical conformations are retained in the lyophilized powder samples. This suggests that this lyophilization process does not yield significant differences in the principal values of the ^{13}C chemical shift tensors. Chemical-shift sideband patterns were analyzed by fitting with the simulated spectra to determine the ^{13}C chemical shift tensors. Table 1 summarizes the ^{13}C chemical shift values and the anisotropies obtained from this study. It is noticed that substantially different principal values were obtained depending on the amino acid residues. Although the orientations of the principal axes were not determined, it is probable that the orientation of δ_{22} is close to the C=O bond direction as observed in simple peptides (Separovic et al., 1990).

Measurement of interatomic distance between [1-^{13}C]Val^{8} and [^{15}N]Leu^{13}

Interatomic distance of carbonyl carbon of Val^{8} and amide nitrogen of Leu^{13} was measured by means of the REDOR method (Gullion and Schaefer, 1989) for the lyophilized powder sample as shown in Fig. 8. In this experiment, we have observed ^{15}N-REDOR and full echo spectra, because the background signals due to natural abundance nuclei can be neglected (Naito et al., 1994). After the experimentally obtained $\Delta S/S_0$ values were plotted as shown in Fig. 8 *b*, the best-fit curve was calculated by considering the effect of finite pulse length to obtain the interatomic distance accurately (Naito et al., 1996). Finally the interatomic distance was determined to be 4.8 ± 0.2 Å. As is discussed later, this value

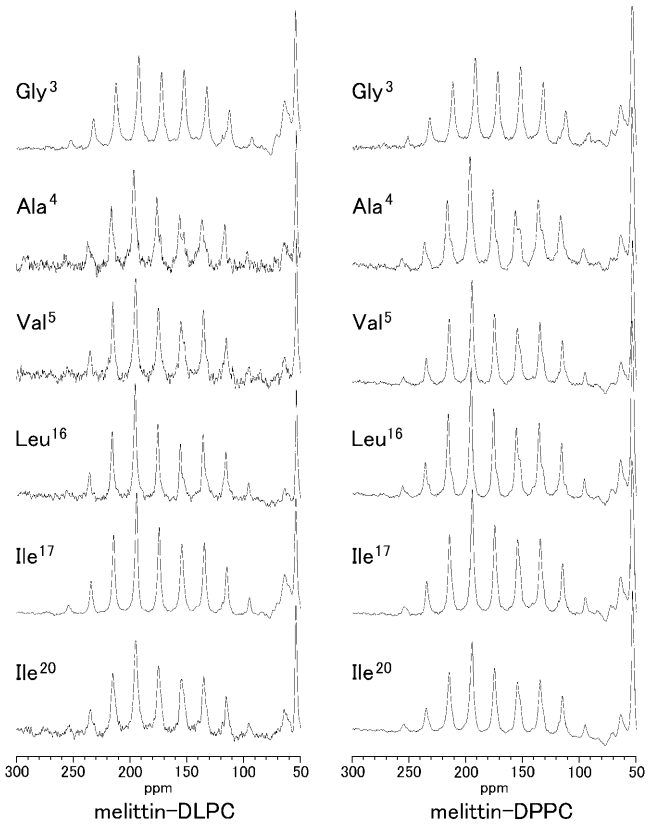

FIGURE 7 ^{13}C-NMR spectra of lyophilized melittin-DLPC and melittin-DPPC bilayer systems using CP-MAS with the spinning frequency of 2 kHz. 4788–33,628 transients were accumulated for the spectra.

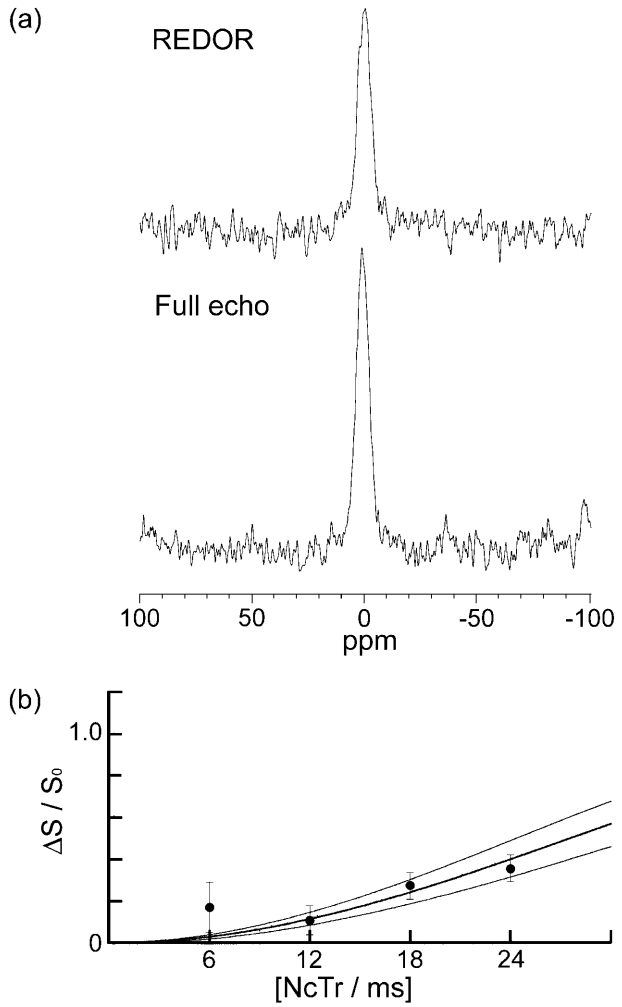

FIGURE 8 (*a*) ^{15}N-REDOR and full echo spectra of [1-^{13}C]Val^{8}, [^{15}N]Leu-melittin in a lyophilized DPPC bilayer system at *NcTr* of 18 ms (9000 transients). (*b*) A plot of $\Delta S/S_0$ against *NcTr* values and the best fit curve indicating the interatomic distance to be 4.8 Å.

provides information for a bending α-helical structure of melittin bound to lecithin bilayers.

DISCUSSION

Analysis of dynamic structures of melittin molecules bound to magnetically oriented vesicles

It is important to reveal the membrane-bound structures of peptides that exhibit their activities by binding to lipid bilayers, if one is to understand the interactions between peptides and lipids. In solid-state NMR studies, membrane-bound structures of peptides have been mostly investigated using mechanically oriented bilayer systems where the bilayers are aligned between glass plates (Nicholson et al., 1987). The structure of melittin was analyzed to be a *trans*-membrane α-helix using mechanically oriented bilayer systems (Smith et al., 1994). However, the melittin molecule did not exhibit its activity as fusion, disruption, or channel formation on membrane in the systems. We believe that insufficient hydration restricts the mobility of the lipid on the glass plate. Experiments with magnetically oriented vesicles dispersed with excess hydration are thus reasonable to determine the active structure and to understand the mechanism of membrane fusion and disruption by melittin.

^{13}C-NMR signals of the carbonyl carbons of the membrane-bound melittin molecules exhibit the chemical shift anisotropies of ~150 ppm when the peptide is immobilized, as shown in Fig. 7 and Table 1. We have proposed that dynamic structures of melittin molecules bound to membranes under the fusion condition can be revealed by analyzing how these large anisotropies are averaged by the motion (Naito et al., 2000). Since anisotropy of magnetic susceptibility of a lecithin is negative, the acyl chains orient perpendicularly to the magnetic field (Boroske and Helfrich, 1978). Thus, when giant vesicles are formed as a result of fusion induced by melittin in the magnetic field, they spontaneously orient the membrane planes parallel to the magnetic field by forming elongated vesicles. Therefore, determining the direction of the rotation axis of melittin with

respect to the oriented vesicle makes it possible to analyze a high-resolution dynamic structure of the peptide bound to the membrane in the mobile system as described below. We therefore developed an approach of analyses of the anisotropic ^{13}C chemical shift interactions for backbone carbonyl carbons of peptides bound to membranes. As shown in Fig. 9, Euler rotations following the convention of Rose (1957) were utilized to transform the ^{13}C chemical shift tensors from the principal-axis frame (PAF) to the helical molecular frame (HMF), and consecutively to the molecular rotating frame (MRF) and finally to the laboratory frame (LF) using the three-step transformation for analyses of the dynamic structures of melittin bound to membranes. Assuming that the δ_{22} axis of the carbonyl carbon is parallel to the helical axis, the Z axis, of melittin (Fig. 9 *a*) for a transformation from the PAF (δ_{11}, δ_{22}, δ_{33}) to the HMF (X, Y, Z), the matrix R_1 of the Euler rotation is given by

$$R_1(\alpha', \beta', \gamma') = R_1(\pi/2, \pi/2, \gamma - \pi/2) = \begin{bmatrix} \cos\gamma & 0 & -\sin\gamma \\ -\sin\gamma & 0 & -\cos\gamma \\ 0 & 1 & 0 \end{bmatrix}, \quad (2)$$

where γ is a constant and the helical axis is directed from the N- to C-terminus. When the helical axis rotates about the Z' axis at a constant tilt angle of ζ to the rotation axis (Fig. 9 *b*), for a transformation from the HMF to the MRF (X', Y', Z'), the matrix R_2 of the Euler rotation is given by

$$R_2(\alpha'', \beta'', \gamma'') = R_2(0, \zeta, \theta) = \begin{bmatrix} \cos\zeta\cos\theta & \sin\theta & -\sin\zeta\cos\theta \\ -\cos\zeta\sin\theta & \cos\theta & \sin\zeta\sin\theta \\ \sin\zeta & 0 & \cos\zeta \end{bmatrix}, \quad (3)$$

where θ varies continuously with a rotational motion at the Z' axis. It is emphasized that the direction of the tilt angle is important to determine the interhelical angle in the case where more than two helices exist in the same molecule. If the rotation axis inclines χ to the magnetic field, the z axis (Fig. 9 *c*), for a transformation from the MRF to the LF (x, y, z) the matrix R_3 of the Euler rotation is given by

$$R_3(\alpha''', \beta''', \gamma''') = R_3(\phi, \chi, 0). \quad (4)$$

Here, ϕ is an arbitrary constant under the static condition, and $\phi = \pi/2$ is chosen accordingly—

$$R_3(\alpha''', \beta''', \gamma''') = R_3(\pi/2, \chi, 0) = \begin{bmatrix} 0 & \cos\chi & -\sin\chi \\ -1 & 0 & 0 \\ 0 & \sin\chi & \cos\chi \end{bmatrix}. \quad (4')$$

Consequently, a rotation matrix of $R = R_3R_2R_1$ transforms the chemical shift tensor from the PAF to the LF, as

$$\tilde{\delta}^{LF} = R \cdot \tilde{\delta}^{PAF} \cdot R^{-1}. \quad (5)$$

When the rotation axis inclines 90° to the magnetic field, the observed chemical shift value $(\delta_{zz})_{\chi=\pi/2} = \delta_\perp$ is expressed as

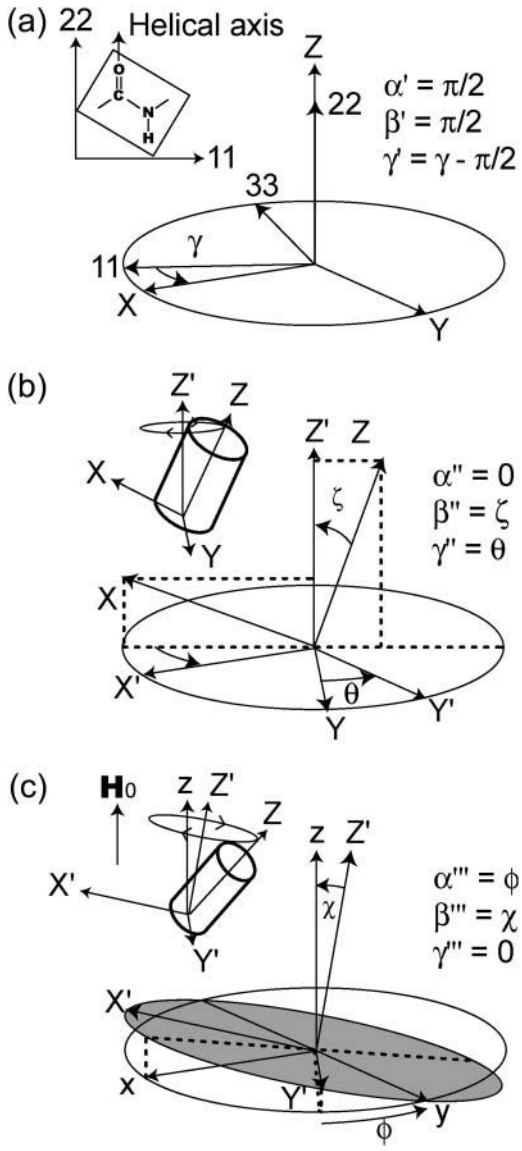

FIGURE 9 Euler rotations for description of the rotational motion of melittin bound to the membrane. (*a*) Rotation from the principal-axis frame (PAF) to the helical molecular frame (HMF). (*b*) Rotation from the HMF to the molecular rotation frame (MRF). (*c*) Rotation from the MRF to the laboratory frame (LF).

$$(\delta_{zz})_{\chi=\pi/2} = \sin^2\theta\{\cos^2\zeta(\delta_{11}\cos^2\gamma + \delta_{33}\sin^2\gamma - \delta_{22}) - (\delta_{11}\sin^2\gamma + \delta_{33}\cos^2\gamma - \delta_{22})\} + \frac{1}{2}\sin 2\theta\cos\zeta\sin 2\gamma(\delta_{11} - \delta_{33}) + \delta_{11}\sin^2\gamma + \delta_{33}\cos^2\gamma. \quad (6)$$

On the other hand, when the rotation axis inclines 0° to the magnetic field, the observed chemical shift value $(\delta_{zz})_{\chi=0} = \delta_{\|}$ is expressed as

$$(\delta_{zz})_{\chi=0} = -\cos^2\zeta(\delta_{11}\cos^2\gamma + \delta_{33}\sin^2\gamma - \delta_{22}) + (\delta_{11}\cos^2\gamma + \delta_{33}\sin^2\gamma). \quad (7)$$

The chemical shift anisotropy, $\Delta\delta = \delta_{\|} - \delta_{\perp}$, is obtained by combining Eqs. 6 and 7 as

$$\Delta\delta = \{(\delta_{11}\cos^2\gamma + \delta_{33}\sin^2\gamma) - \cos^2\zeta(\delta_{11}\cos^2\gamma + \delta_{33}\sin^2\gamma - \delta_{22})\} - \sin^2\theta\{\cos^2\zeta(\delta_{11}\cos^2\gamma + \delta_{33}\sin^2\gamma - \delta_{22}) - (\delta_{11}\sin^2\gamma + \delta_{33}\cos^2\gamma - \delta_{22})\} - \frac{1}{2}\sin 2\theta\cos\zeta\sin 2\gamma(\delta_{11} - \delta_{33}) - \delta_{11}\sin^2\gamma - \delta_{33}\cos^2\gamma. \quad (8)$$

Here, functions of θ can be averaged over a cycle when the helical axis rotates rapidly about the axis parallel to the membrane normal that corresponds to the Z' axis. In this case, we obtain an expression where the averaged anisotropy depends on the phase angle, γ, of the peptide plane about the helical axis, and the tilt angle, ζ, of the helical axis from the rotation axis as

$$\overline{\Delta\delta} = \frac{3}{2}\sin^2\zeta(\delta_{11}\cos^2\gamma + \delta_{33}\sin^2\gamma - \delta_{22}) + \left(\delta_{22} - \frac{\delta_{11} + \delta_{33}}{2}\right) = \frac{3}{2}\sin^2\zeta(\delta_{11}\cos^2\gamma + \delta_{33}\sin^2\gamma - \delta_{22}) + (\overline{\Delta\delta})_{\zeta=0}, \quad (9)$$

where

$$(\overline{\Delta\delta})_{\zeta=0} = \delta_{22} - \frac{\delta_{11} + \delta_{33}}{2}. \quad (10)$$

Since the C- and N-terminal regions of melittin adopt α-helical structures, the phase angle, γ, varies by $-100°$ per consecutive residue in the direction toward the C-terminus. Eq. 9 indicates that $\overline{\Delta\delta}$ of the carbonyl carbon can be oscillatorily changed as a function of γ along the consecutive amino acid sequence in the α-helical region. The amplitude of the oscillation depends on the tilt angle ζ. We call this behavior a *chemical-shift oscillation*. This behavior can be compared with the PISA wheel experiments, where the ^{15}N-^{1}H dipolar and ^{15}N chemical shift interactions are the functions of γ and ζ (Marassi and Opella, 2000; Wang et al., 2000). To determine the tilt angle, ζ, and the phase angle, γ, for α-helical rods of the N- and C-terminals individually, we take root mean-square deviations (RMSDs) of the ^{13}C chemical shift anisotropies obtained from the three amino acid residues for the N-terminal helical rod (Gly^3, Ala^4, and Val^5) and the C-terminal helical rod (Leu^{16}, Ile^{17}, and Ile^{20}) as

$$RMSD = \left[\sum_{i=1}^{3}\{(\Delta\delta_{obs})_i - (\Delta\delta_{cal})_i\}^2/3\right]^{\frac{1}{2}}. \quad (11)$$

The least RMSD provides the phase angles, γ_{G3} and γ_{L16}, of the peptide plane at Gly^3 and Leu^{16} and the tilt angles, ζ_N and ζ_C, of the helical axes of the N- and C-termini from the membrane-normal, respectively. Once γ_{G3} and γ_{L16} are determined, the other phase angle in each rod is simultaneously determined by considering the structure of α-helix.

We also consider a case where the membrane-bound melittin also rotates about the helical axis. In this case, the Euler angle α'' is set to a time-dependent variable, ε, instead of 0 in the rotation matrix transforming the HMF into the MRF, and the X,Y plane rotates rapidly around the helical axis. Because time-averaging of ε-dependent terms simultaneously causes functions of γ to be averaged, $\overline{\Delta\delta}$ becomes independent of γ. In the ^{13}C-NMR experiments, $\overline{\Delta\delta}$ exhibited such large changes that the sign was altered between the carbonyl carbons observed at neighboring residues as shown in Table 1. These results imply that the helices do not rotate about the helical axes but rotate about the membrane normal, and α'' must thus be a constant.

Fig. 10 shows RMSD contour plots of the ^{13}C chemical shift anisotropies, where RMSD is plotted against γ as abscissa and ζ as ordinate. Owing to the symmetry property of the Eq. 9, the relations

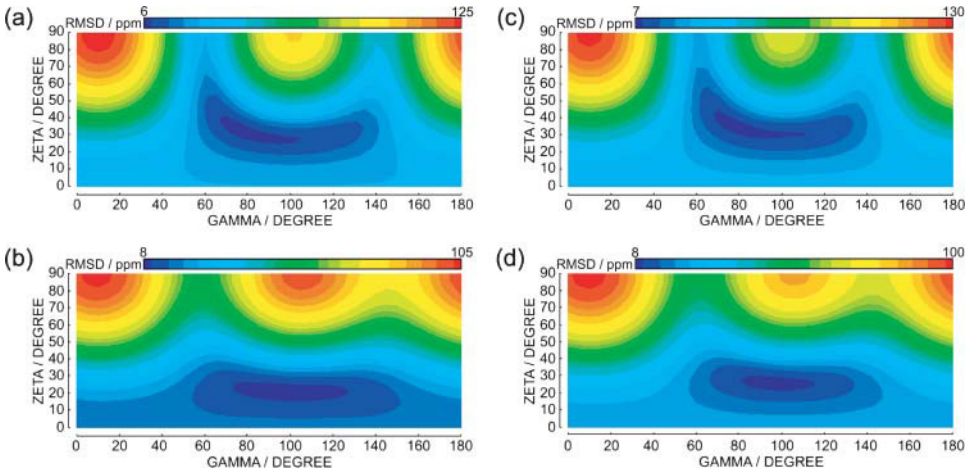

FIGURE 10 Contour plots of RMSD of experimental and theoretical ^{13}C chemical shift anisotropies. (*a*, *c*) Contour plots for the N-terminal helix of melittin bound to DLPC and DPPC vesicles, respectively. (*b*, *d*) Contour plots for the C-terminal helix of melittin bound to DLPC and DPPC vesicles, respectively. RMSD values increase from blue to red.

$$\begin{aligned} RMSD(\gamma,\zeta) &= RMSD(\gamma-180^\circ,\zeta) \\ &= RMSD(\gamma-180^\circ,-\zeta) \\ &= RMSD(\gamma,-\zeta) \end{aligned} \tag{12}$$

are fulfilled. For the N- and C-terminal helices in the melittin-DLPC bilayer systems, the least RMSD indicates

$$\begin{aligned} (\gamma_{G3},\zeta_N)_{DLPC} &= (+76^\circ,\pm33^\circ)_{DLPC} \\ &\text{or}\quad (-104^\circ,\pm33^\circ)_{DLPC} \end{aligned} \tag{13}$$

and

$$\begin{aligned} (\gamma_{L16},\zeta_C)_{DLPC} &= (+99^\circ,\pm21^\circ)_{DLPC} \\ &\text{or}\quad (-81^\circ,\pm21^\circ)_{DLPC}, \end{aligned} \tag{14}$$

respectively. For the N- and C-terminal helices in the melittin-DPPC bilayer systems, the least RMSD indicates

$$\begin{aligned} (\gamma_{G3},\zeta_N)_{DPPC} &= (+76^\circ,\pm36^\circ)_{DPPC} \\ &\text{or}\quad (-104^\circ,\pm36^\circ)_{DPPC} \end{aligned} \tag{15}$$

and

$$\begin{aligned} (\gamma_{L16},\zeta_C)_{DPPC} &= (+98^\circ,\pm25^\circ)_{DPPC} \\ &\text{or}\quad (-82^\circ,\pm25^\circ)_{DPPC}, \end{aligned} \tag{16}$$

respectively. Since Thr^{10} cannot form a hydrogen bond to Pro^{14}, and the MAS experiments (Figs. 4 and 5) and our previous study (Naito et al., 2000) showed that Gly^3, Ala^4, Val^5, Gly^{12}, Ala^{15}, Leu^{16}, Ile^{17}, and Ile^{20} adopt α-helical conformations, we assume that Thr^{11} locates as a boundary between Gly^1-Thr^{10} and Gly^{12}-Gln^{26}, and that the two regions adopt typical α-helical structures. The two possible structures of melittin bound to the DPPC vesicles were shown in Fig. 11 out of 16 possible structures. In the case of extended structure shown in Fig. 11 *a*, the ^{13}C–^{15}N interatomic distance between [1-^{13}C]Val^8 and [^{15}N]Leu^{13} is expected to be longer than 6.9 Å. On the other hand, this distance is expected to be 4.8 Å in the case of bend structure shown in Fig. 11 *b*. In our previous report, NMR experiments could not distinguish such two structures as shown in Fig. 10, *a* and *b* (Naito et al., 2000). We have determined the interatomic distance between [1-^{13}C]Val^8 and [^{15}N]Leu^{13} for melittin bound to lyophilized DPPC bilayers by means of a REDOR method. The distance was determined to be 4.8 ± 0.2 Å, clearly indicating that the structure with

$$\begin{aligned} (\gamma_{G3},\zeta_N)_{DPPC} &= (+76^\circ\pm6^\circ,-36^\circ\pm3^\circ)_{DPPC} \quad\text{and} \\ (\gamma_{L16},\zeta_C)_{DPPC} &= (-82^\circ\pm16^\circ,+25^\circ\pm3^\circ)_{DPPC}, \end{aligned} \tag{17}$$

as illustrated in Fig. 11 *b*, is the actual structure and the other possible structures were ruled out. When melittin adopts the structure shown in Fig. 11 *b*, it agrees well with the structure found by the x-ray diffraction studies (Terwilliger and Eisenberg, 1982; Terwilliger et al., 1982). Namely the carbonyl group at Val^8 can form hydrogen bond to the amide group at Leu^{13}, and this allows the molecule to behave as a rigid body in membrane. Also for the case of dynamic structure of melittin bound to the DLPC membrane, we finally obtain

$$\begin{aligned} (\gamma_{G3},\zeta_N)_{DLPC} &= (+76^\circ\pm5^\circ,-33^\circ\pm3^\circ)_{DLPC} \quad\text{and} \\ (\gamma_{L16},\zeta_C)_{DLPC} &= (-81^\circ\pm24^\circ,\ +21^\circ\pm5^\circ)_{DLPC} \end{aligned} \tag{18}$$

for the actual structure.

Interestingly, alteration of the lipid acyl-chain length brought about significant differences in the tilt angles, ζ_N and ζ_C, rather than the phase angles, γ_{G3} and γ_{L16}. Since Gly^{12} of melittin bound to the DMPC membrane adopts a typical α-helical conformation under a fusion condition (Naito et al., 2000), the kink angle of the helical molecule is attributed to the torsion angles of predominantly the vicinity of Thr^{11} that is the linking position of the two helical rods. The interhelical

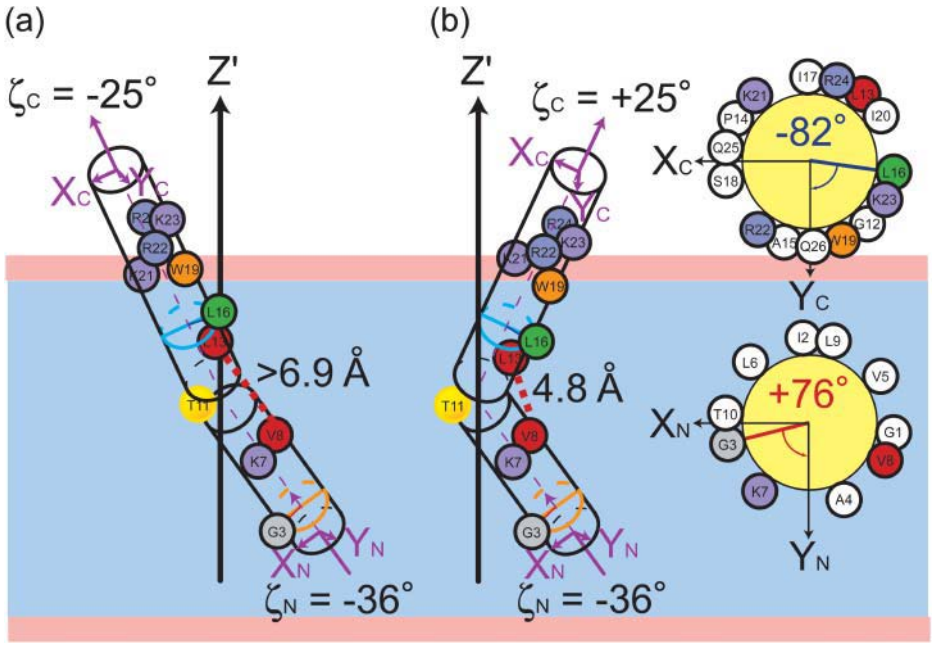

FIGURE 11 Schematic representations of the possible structures of melittin bound to the DPPC vesicle from the analyses of the ^{13}C chemical shift anisotropies. (*a*) $(\gamma_{G3}, \zeta_N) = (+76°, -36°)$ and $(\gamma_{L16}, \zeta_C) = (-82°, -25°)$. (*b*) $(\gamma_{G3}, \zeta_N) = (+76°, -36°)$ and $(\gamma_{L16}, \zeta_C) = (-82°, +25°)$. Structure *b* is proved to be the actual structure based on the interatomic distance of 4.8 ± 0.2 Å, between [1-^{13}C]Val^8 and [^{15}N]Leu^{13} of melittin bound to the DPPC bilayers, determined by the REDOR measurements. The helical wheel representations were illustrated in the HMF, which is identical with that defined in Fig. 9 *b*. The *Z′* axis is the rotation axis of a melittin molecule, which is parallel to the membrane normal.

angle of melittin changed from 126° ± 8° in DLPC to 119° ± 6° in DPPC through the torsion angles of Thr^{11} as a result of altering the acyl groups of the lipid forming the bilayer from lauroyl to palmitoyl. We could detect this small change as significant differences between the chemical shift values, δ_{obs}, observed under the oriented conditions as summarized in Table 1. These angles are slightly smaller than those of melittin in the lyophilized powder and the hydrated gel phase of DTPC (Lam et al., 2001). Conversely, the experiments indicate that our approach, as proposed in this study, is useful for analyses of structures and dynamics of peptides bound to dynamic membranes. It is also emphasized that this approach can determine not only the structure of membrane-bound molecules but also the orientation with respect to the membrane.

Mechanism of membrane fusion induced by melittin

It is demonstrated that alteration of lipid-acyl chain length causes a slight change in the interhelical angle of melittin (126° ± 8° and 119° ± 6° for DLPC and DPPC, respectively). Lis et al. (1982) reported that an increase of acyl chain length of lipid molecule increases the bilayer thickness in the liquid crystalline states (Lis et al., 1982). It is of interest to note that distances between the termini of melittin are estimated to be ~34 and ~33 Å in the DLPC and DPPC bilayer systems, respectively, where melittin adopts the helical structure with 5.4 Å pitch as shown in Fig. 11 *b*. On the other hand, bilayer thicknesses of DLPC and DPPC bilayers are 30.0 and 34.2 Å, respectively (Lis et al., 1982). It is therefore possible for melittin molecules to take *trans*-membrane structures in DLPC and DPPC bilayers. However, the hydrophilic residues of K^{21}-R^{24} may make one cycle of α-helix and locate in the hydrophilic region of lecithin bilayers by orienting parallel to the membrane plane as shown in Fig. 11 *b*. Tryptophan residue has also been reported to show an interfacial anchoring property (de Planque et al., 2003). Thus, W^{19} may locate itself at the interfacial regions of lecithin bilayers. It is therefore reasonable to predict that the consecutive basic residues are located in the polar region. Consequently, the N-terminus of melittin cannot reach to the water-lipid interface, penetrating the hydrophobic core of the bilayers as a pseudo-*trans*-membrane structure. As length of the acyl chain increases, interactions between the hydrophobic bulky side chains of such residues as Ala, Ile, Leu, and Val inside of the bend and the hydrophobic core of lipid bilayer increases to cause the slight change in the interhelical angle. It is discussed that the incomplete insertion of the N-terminal α-helix of melittin may cause a great disorder in the lipid bilayer surface on the N-terminal side. The surface disorder induces lipid mixing between adjacent vesicles, thereby membrane fusion occurs.

CONCLUSIONS

It was demonstrated that the magnetically oriented vesicle systems (MOVS) were formed in the melittin-lecithin bilayer systems. Using MOVS, dynamic structure of melittin bound to the lipid bilayer was found as a pseudo-*trans*-membrane bend structure, and melittin molecules rotate rapidly about the axis parallel to the bilayer normal. Furthermore, we could experimentally detect the small change in the tilt angles of the helical axes of the N- and C-terminal helices from the

membrane normal as significant differences between the chemical shift values observed under the conditions where the membrane plane spontaneously orient parallel to the magnetic field. Consequently, detailed analyses of ^{13}C chemical shift interactions of carbonyl carbons revealed the interhelical angles of melittin molecules bound to the DLPC and DPPC vesicles to be 126° and 119°, respectively. Although there are certain differences in the dynamic structures of melittin molecules bound to membranes depending on the membrane systems, melittin exhibits common activities on DLPC, DMPC, and DPPC bilayers such as membrane fusion (above T_c) and disruption (below T_c). In this study, the membrane fusion mechanism can be attributed to the fact that the melittin strongly binds to the vesicle with the pseudo-*trans*-membrane structure and orientation, which causes disorder of the lipid bilayer surface.

This work was supported, in part, by a Grant-in-Aid for Scientific Research on Priority Areas (13024263) from the Ministry of Culture, Sports, Science and Technology of Japan.

REFERENCES

Altenbach, C., W. Froncisz, J. S. Hyde, and W. L. Hubbell. 1989. Conformation of spin-labeled melittin at membrane surfaces investigated by pulse saturation recovery and continuous wave power saturation electron paramagnetic resonance. *Biophys. J.* 56:1183–1191.

Anderson, D., T. C. Terwilliger, W. Wickner, and D. Eisenberg. 1980. Melittin forms crystals which are suitable for high resolution x-ray structural analysis and which reveal a molecular twofold axis of symmetry. *J. Biol. Chem.* 255:2578–2582.

Bazzo, R., M. J. Tappin, A. Pastore, T. S. Harvey, J. A. Carver, and I. D. Campbell. 1988. The structure of melittin. A ^{1}H-NMR study in methanol. *Eur. J. Biochem.* 173:139–146.

Bello, J., H. R. Bello, and E. Granados. 1982. Conformation and aggregation of melittin: dependence on pH and concentration. *Biochemistry.* 21:461–465.

Boroske, E., and W. Helfrich. 1978. Magnetic anisotropy of egg lecithin membranes. *Biophys. J.* 24:863–868.

Brauner, J. W., R. Mendelsohn, and F. G. Prendergast. 1987. Attenuated total reflectance Fourier transform infrared studies of the interaction of melittin, two fragments of melittin, and δ-hemolysin with phosphatidylcholines. *Biochemistry.* 26:8151–8158.

Dawson, C. R., A. F. Drake, J. Helliwell, and R. C. Hider. 1978. The interaction of bee melittin with lipid bilayer membranes. *Biochim. Biophys. Acta.* 510:75–86.

de Planque, M. R. R., B. B. Bonev, J. A. A. Demmers, D. V. Greathouse, G. E. Koeppe, II, F. Separovic, A. Watts, and J. A. Killian.2003. Interfacial anchor properties of tryptophan residues in *trans*-membrane peptides can dominate over hydrophobic matching effects in peptide-lipid interactions. *Biochemistry.* 47:5341–5348.

Dufourcq, J., J.-F. Faucon, G. Fourche, J.-L. Dasseux, M. Le Maire, and T. Gulik-Krzywicki. 1986. Morphological changes of phosphatidylcholine bilayers induced by melittin: vesicularization, fusion, discoidal particles. *Biochim. Biophys. Acta.* 859:33–48.

Eytan, G. D., and T. Almary. 1983. Melittin-induced fusion of acidic liposomes. *FEBS Lett.* 156:29–32.

Faucon, J.-F., J.-M. Bonmatin, J. Dufourcq, and E. J. Dufourc. 1995. Acyl-chain-length dependence in the stability of melittin-phosphatidylcholine complexes. A light scattering and ^{31}P-NMR study. *Biochim. Biophys. Acta.* 1234:235–243.

Gullion, T., and J. Schaefer. 1989. Rotational echo double-resonance NMR. *J. Magn. Reson.* 81:196–200.

Habermann, E. 1972. Bee and wasp venoms. *Science.* 177:314–322.

Habermann, E., and J. Jentsch. 1967. Sequenzanalyse des melittins aus den tryptischen und peptischen spaltstücken. *Hoppe-Seyler's Z. Physiol. Chem.* 348:37–50.

Inagaki, F., I. Shimada, K. Kawaguchi, M. Hirano, I. Terasawa, T. Ikura, and N. Gō. 1989. Structure of melittin bound to perdeuterated dodecylphosphocholine micelles as studied by two-dimensional NMR and distance geometry calculations. *Biochemistry.* 28:5985–5991.

Kempf, C., R. D. Klausner, J. N. Weinstein, J. Van Renswoude, M. Pincus, and R. Blumenthal. 1982. Voltage-dependent *trans*-bilayer orientation of melittin. *J. Biol. Chem.* 257:2469–2476.

Kings, D. S., C. G. Fields, and G. B. Fields. 1990. A cleavage method which minimizes side reactions following Fmoc solid phase peptide synthesis. *Int. J. Pept. Protein Res.* 36:255–266.

Knöppel, E., D. Eisenberg, and W. Wickner. 1979. Interactions of melittin, a protein model, with detergents. *Biochemistry.* 18:4177–4181.

Lam, Y.-H., S. R. Wassall, C. I. Morton, R. Smith, and F. Separovic. 2001. Solid-state NMR structure determination of melittin in a lipid environment. *Biophys. J.* 81:2752–2764.

Lis, L. J., M. McAlister, N. Fuller, R. P. Rand, and V. A. Parsegian. 1982. Interactions between neutral phospholipid bilayer membranes. *Biophys. J.* 37:657–666.

Marassi, F. M., and S. J. Opella. 2000. A solid-state NMR index of helical membrane protein structure and topology. *J. Magn. Reson.* 144:150–155.

Mollay, C., and G. Kreil. 1974. Enhancement of bee venom phospholipase A_2 activity by melittin, direct lytic factor from cobra venom and polymyxin B. *FEBS Lett.* 46:141–144.

Mollay, C., G. Kreil, and H. Berger. 1976. Action of phospholipases on the cytoplasmic membrane of *Escherichia coli*. *Biochim. Biophys. Acta.* 426:317–324.

Morgan, C. G., H. Williamson, S. Fuller, and B. Hudson. 1983. Melittin induces fusion of unilamellar phospholipid vesicles. *Biochim. Biophys. Acta.* 732:668–674.

Naito, A., T. Nagao, K. Norisada, T. Mizuno, S. Tuzi, and H. Saitô. 2000. Conformation and dynamics of melittin bound to magnetically oriented lipid bilayers by solid-state ^{31}P- and ^{13}C-NMR spectroscopy. *Biophys. J.* 78:2405–2417.

Naito, A., T. Nagao, M. Obata, Y. Shindo, M. Okamoto, S. Yokoyama, S. Tuzi, and H. Saitô. 2002. Dynorphin-induced magnetic ordering in lipid bilayers as studied by ^{31}P-NMR spectroscopy. *Biochim. Biophys. Acta.* 1558:34–44.

Naito, A., K. Nishimura, S. Kimura, M. Aida, N. Yasuoka, S. Tuzi, and H. Saitô. 1996. Determination of the three-dimensional structure of a new crystalline form of *n*-acetyl-Pro-Gly-Phe as revealed by ^{13}C REDOR, x-ray diffraction, and molecular dynamics calculation. *J. Phys. Chem. B.* 100:14995–15004.

Naito, A., K. Nishimura, S. Tuzi, and H. Saitô. 1994. Inter- and intramolecular contributions of neighboring dipolar pairs to the precise determination of interatomic distances in a simple [^{13}C, ^{15}N]-peptide by ^{13}C, ^{15}N-REDOR NMR spectroscopy. *Chem. Phys. Lett.* 229:506–511.

Nicholson, L. K., F. Moll, T. E. Mixon, P. V. LoGrasso, J. C. Lay, and T. A. Cross. 1987. Solid-state ^{15}N-NMR of oriented lipid bilayer bound gramicidin A′. *Biochemistry.* 26:6621–6626.

Okada, A., K. Wakamatsu, T. Miyazawa, and T. Higashijima. 1994. Vesicle bound conformation of melittin: transferred nuclear Overhauser enhancement analysis in the presence of perdeuterated phosphatidylcholine vesicles. *Biochemistry.* 33:9438–9446.

Paquet, A. 1982. Introduction of 9-fluorenylmethoxycarbonyl, trichloroethoxycarbonyl, and benzyloxycarbonyl amine protecting groups into O-unprotected hydroxyamino acids using succinimidyl carbonates. *Can. J. Chem.* 60:976–980.

Quay, S. C., and C. C. Condie. 1983. Conformational studies of aqueous melittin: thermodynamics parameters of the monomer-tetramer self-association reaction. *Biochemistry.* 22:695–700.

Rose, M. E. 1957. Elementary Theory of Angular Momentum. John Wiley and Sons, New York.

Saitô, H., and I. Ando. 1989. High-resolution solid-state NMR studies of synthetic and biological macromolecules. *Annu. Rep. NMR Spectrosc.* 21:209–290.

Sanders, C. R. 1993. Solid state ^{13}C-NMR of unlabeled phosphatidylcholine bilayers: spectral assignments and measurement of carbon-phosphorus dipolar couplings and ^{13}C chemical shift anisotropies. *Biophys. J.* 64:171–181.

Separovic, F., R. Smith, C. S. Yannoni, and B. A. Cornell. 1990. Molecular sequence effect on the ^{13}C carbonyl chemical shift shielding tensor. *J. Am. Chem. Soc.* 112:8324–8328.

Sessa, G., J. H. Freer, G. Colaccico, and G. Weissmann. 1969. Interaction of a lytic polypeptide, melittin, with lipid membrane systems. *J. Biol. Chem.* 244:3575–3582.

Smith, R., F. Separovic, T. J. Milne, A. Whittaker, F. M. Bennett, B. A. Cornell, and A. Makriyannis. 1994. Structure and orientation of the pore-forming peptide, melittin, in lipid bilayers. *J. Mol. Biol.* 241:456–466.

Talbot, J. C., J. Dufourcq, J. de Bony, J. F. Faucon, and C. Lussan. 1979. Conformational change and self-association of monomeric melittin. *FEBS Lett.* 102:191–193.

Terwilliger, T. C., and D. Eisenberg. 1982. The structure of melittin. *J. Biol. Chem.* 257:6010–6015.

Terwilliger, T. C., L. Weissman, and D. Eisenberg. 1982. The structure of melittin in the form I crystals and its implication for melittin's lytic and surface activities. *Biophys. J.* 37:353–361.

Tosteson, M. T., and D. C. Tosteson. 1981. Melittin forms channels in lipid bilayers. *Biophys. J.* 36:109–116.

Van Dijck, P. W. M., B. De Kruijff, L. L. M. Van Deenen, J. De Gier, and R. A. Demel. 1976. The preference of cholesterol for phosphatidylcholine in mixed phosphatidylcholine-phosphatidylethanolamine bilayers. *Biochim. Biophys. Acta.*. 455:576–587.

Vogel, H., F. Jähnig, V. Hoffmann, and J. Stümpel. 1983. The orientation of melittin in lipid membranes. A polarized infrared spectroscopy study. *Biochim. Biophys. Acta.* 733:201–209.

Yang, L., T. A. Harroun, T. M. Weiss, L. Ding, and H. W. Huang. 2001. Barrel-stave model or toroidal model? A case study on melittin pores. *Biophys. J.* 81:1475–1485.

Wang, J., J. Denny, C. Tian, S. Kim, Y. Mo, F. Kovacs, Z. Song, K. Nishimura, Z. Gan, R. Fu, J. R. Quine, and T. A. Cross. 2000. Imaging membrane protein helical wheels. *J. Magn. Reson.* 144:162–167.